Materials Today Advances 13 (2022) 100199

Contents lists available at ScienceDirect

Materials Today Advances

journal homepage: www.journals.elsevier.com/materials-today-advances/

Combination of photothermal, prodrug and tumor cell camouflage technologies for triple-negative breast cancer treatment

Lirong Zhang [a, 1], Xiaodong Ma [a, b, c, 1], Wenhui Zhou [d, b, c, f, 1], Qiwei Wu [a], Jiaqi Yan [b, c], Xiaoyu Xu [b, c], Bhawana Ghimire [b, c], Jessica M. Rosenholm [b], Jing Feng [d, e, **], Dongqing Wang [a, ***], Hongbo Zhang [b, c, *]

[a] Department of Radiology Affiliated Hospital of Jiangsu University, Zhenjiang, 212001, China
[b] Pharmaceutical Sciences Laboratory, Åbo Akademi University, Turku, 20520, Finland
[c] Turku Bioscience Centre, University of Turku and Åbo Akademi University, Turku, 20520, Finland
[d] Southern Medical University Affiliated Fengxian Hospital, Shanghai, 201499, China
[e] Longgang District People's Hospital of Shenzhen, Shenzhen, 518172, China
[f] Hubei Key Laboratory of Embryonic Stem Cell Research, Taihe Hospital, Hubei University of Medicine, Shiyan, 442000, China

ARTICLE INFO

Article history:
Received 4 October 2021
Received in revised form
4 December 2021
Accepted 7 December 2021
Available online 10 December 2021

Keywords:
Photothermal therapy
Prodrug
Cell camouflage nanoparticles
Combination therapy
Triple negative breast cancer

ABSTRACT

Triple-negative breast cancer (TNBC) remains the most challenging breast cancer subtype. In the presented work, we have combined several emerging technologies to build up a nanoplatform for TNBC treatment: photothermal therapy, prodrug design and tumor cell camouflage formulation. First, we synthesized a paclitaxel (PTX) based prodrug PTX-SS, and then conjugated it to the surface of gold nanorod (Au NR) @ mesoporous silica (MSN) core-shell nanoparticles (Au@MSN-NH_2 NPs). Subsequently, doxorubicin (DOX) was loaded into the Au@PTXSS-MSN NPs and further coated with cell membranes isolated from MDA-MB-231 cells to form cell camouflaged Au@PTXSS-MSN/DOX@CM NPs. The Au@PTXSS-MSN/DOX@CM NPs exhibited very good DOX loading capacity and the prodrug strategy enabled the precise adjustability of PTX-SS loading to achieve the optimized ratio between PTX and DOX to maximize the synergistic effect of these two drugs, as well as enabled GSH-responsive intracellular drug release. More interestingly, the cell membrane coating not only protected the drug from premature release, but also significantly improved the targeting ability of NPs to breast cancer MDA-MB-231 cells. The NPs also showed good photothermal responsiveness with clear improvement in inhibiting MDA-MB-231 cell proliferation under laser irradiation. The *in vivo* studies further confirmed the effectiveness of Au@PTXSS-MSN/DOX@CM NPs on TNBC tumor inhibition in 4T1 cell grafted tumor mice model.

1. Introduction

Triple-negative breast cancer (TNBC) is the most aggressive breast cancer that is accompanied by poor prognosis and high rate of recurrence and metastasis [1]. The using of targeted anti-cancer drugs (such as Herceptin, Lapatinib and Pertuzumab) has dramatically improved the prognosis of breast cancer; however, TNBC still lacks effective therapeutic drugs due to the lack expression of hormone receptors (include estrogen receptor, progesterone receptor and human epidermal growth factor receptor 2), which are widely used for breast cancer targeting therapy [2]. Cell camouflage technologies that utilize cancer cell originating cell membranes to hidden the drug carrier nanoparticles (NPs), have been found to be a good strategy for targeted cancer therapy owing to the extensive homology of the proteins and antigens between the cell membrane and cancer cells, as well as the homing ability of cancer cells [3,4]. For example, Nie [5] has developed a tumor cell membrane coated mesoporous silica NPs (MSNs) loaded with doxorubicin and the poly (ADP-ribose) polymerase inhibitor, which exhibited a stronger antitumor activity than Doxil. Sun [6] also reported a 4T1 cell membrane coated and paclitaxel loaded

* Corresponding author. Pharmaceutical Sciences Laboratory, Åbo Akademi University, Turku, 20520, Finland.
** Corresponding author. Southern Medical University Affiliated Fengxian Hospital, Shanghai, 201499, China.
*** Corresponding author.
E-mail addresses: fengjing71921@163.com (J. Feng), wangdongqing71@163.com (D. Wang), hongbo.zhang@abo.fi (H. Zhang).
[1] These authors contribute equally to this work.

https://doi.org/10.1016/j.mtadv.2021.100199

nanoparticle, which displayed significant targeting ability against homotypic primary tumor and metastases. Therefore, the cell camouflage technologies hold great potential for TNBC targeting therapy.

Prodrugs refer to pharmacological compounds that are temporarily or permanently bonded to certain chemical groups, fragments or molecules through covalent bonding [7,8]. The prodrugs can be converted to functional substance when subject to certain stimuli in the body, while they have no or limited activity in vitro [9]. This methodology has been widely used in drug design to improve bioavailability, targeting, and also to reduce the side effects of the drugs [10]. For example, the binding of camptothecin (CPT) and curcumin (CCM) prodrugs with albumin-based NPs has greatly improved the therapeutic efficiency in subcutaneous 4 T1 and HepG2 tumor models [11]. Hattori [12] also reported that two developed decitabine (DAC) based prodrugs for DNA-demethylating exhibited much better metabolic stability with reduced cytotoxicity. In addition, another attractive advantage of prodrugs is their ability to stimuli-responsiveness. For example, hydrophilic polyethylene glycol (PEG) and amphiphilic cationic mitoxantrone (MTO) formed pH-responsive polymer-prodrug NPs has been used to load siRNA to achieve synergistic effect and pH responsive drug release for cancer therapy [13]. Prodrugs are also considered as one of the best solutions to TNBC. For example, Umeh-Garcia developed an engineered miR-127 prodrug, which shows great ability of growth inhibition and anti-metastasis ability in TNBC [14]. Similarly, another developed platinum prodrug also shows increased sensitivity of TNBC cells to cisplatin [15].

Photothermal therapy (PTT) is a main method for cancer physical therapy. PTT mainly uses photothermal conversion materials to generate instantaneous high temperature under the irradiation of an additional light source (mainly near-infrared light (NIR)) to kill cancer cells [16]. The main advantages of PTT are that significant therapeutic effect can be achieved along with barely any side effects through multiple consecutive short-term treatments; and most importantly, the pain caused by treatment can be greatly reduced [17]. Gold NPs (Au NPs), including gold nanorods (Au NRs) and nanoshells have always been considered as good materials for PTT owing to their perfect heat production ability when excited by NIR [18]. Au NPs also have been regarded and widely used as excellent NPs for drugs or other small molecules delivery, as well as bioimaging owing to their high electron density, dielectric properties and catalytic activity [19–21]. However, due to the small surface-to-volume ratio of Au NPs, their drug-carrying capacity is limited [21]. Therefore, lots of efforts have been done for the increasing of drug loading capacity of Au NPs. Among them, the encapsulation of Au NRs with MSNs is one of the most widely used strategy to expand the drug loading capacity of Au NPs. MSNs are NPs with controllable particle size and shape and formed by biocompatible mesoporous silica nanomaterials. They have acquired increasing interest of potential application in drug and gene delivery owing to their multiscale pore structures, high surface-to-volume ratio and also modifiable surface [22–24]. It has been reported that MSN-coated Au NRs (Au@MSN-NH_2) exhibited not only combined chemotherapy and PTT, but also stimuli-induced drug release [25–27]. Thus, Au NRs can be served as a talent candidate for multi-methods based combinational treatment of TNBC.

In this work (as shown in Scheme 1), we have developed a paclitaxel (PTX) based prodrug, which is further conjugated to the surface of photothermal responsive Au@MSN-NH_2 NPs through a disulfide bond linker. Subsequently, the chemotherapeutic doxorubicin (DOX) was loaded at an optimized DOX/PTX ratio to generate synergistic effect between the two drugs. Furthermore, the nanoparticle was coated with MDA-MB-231 derived cell membranes to improve the tumor cell targeting efficiency.

2. Results and discussion

2.1. Preparation and characterization of Au NRs and Au@MSN-NH_2 NPs

To begin with this work, we are planned to develop a photothermal responsive drug delivery nanocarrier that can be used for PTT and chemotherapy combined treatment of TNBC. It has been established that the best particle size of Au NPs for PTT and imaging is larger than 50 nm. Therefore, we primarily used the seed mediated growth methods in cetyltrimethylammonium bromide (CTAB) presented aqueous solution at room temperature to form the Au NRs as reported before [28]. As shown in Fig. 1A, the synthesized Au NRs were acquired with a nanorodes morphology and the particle size was 57.3 ± 4.4 nm. In order to increase the chemotherapeutic drug loading capacity of the prepared Au NRs, we utilized MSN to form a porous shell structure on top of the Au NRs through another CTAB mediated seed-growth methods. As shown in Fig. 1B, the porous structure of MSN outside of the Au@MSN-NH_2 NPs was obviously observed in the TEM imaging, and the particle size was increased up to 102.9 ± 1.2 nm (Fig. 1D) while the zeta-potential and PDI were 11.4 ± 0.2 mV and 0.11 ± 0.01 (Supplementary Fig. 4A and B) when dispersed in deionized water.

2.2. PTX-SS-COOH synthesis and characterization

Strategies for combined drug delivery has always been considered as good methods for solving the problem of cancer drug resistance [29,30]. For example, the codelivery of PTX and curcumin by an amphiphilic copolymers have been reported to have the ability of reversing ovarian cancer drug resistance [31], and the codelivery of nucleic acid drugs and chemotherapeutics have also been confirmed to have the ability of reversing the drug resistance in colon cancer [32]. However, the co-delivery of both hydrophilic and lipophilic drugs within one nanocarrier remains a big challenge [33]. Moreover, the ratio of combined drugs loading is a very important factor for combined drug therapy. In order to improve the drug-carrying capacity of our previously synthesized Au@MSN-NH2 NPs and realize the controllable co-delivery, as well as reduce the toxic side effects of the used chemotherapeutic drugs, we firstly made PTX into the prodrug form of PTX-S-S-COOH by a redox-sensitive linker, which was then bound to MSN-NH_2. As shown in Fig. 2A, an esterification reaction was firstly performed between PTX and the redox-sensitive linker to form PTX-SS-COOH by a one-step reaction in the presence of DTDP, which is a commonly used redox-sensitive linker that promotes the release of paclitaxel under highly reducing conditions in cells. As shown in Fig. 2B, the aliphatic proton peak of PTX was in the range of 1.0–2.5 ppm. Among all of the PTX hydroxyl groups, the one attached to C-2′ is more likely to react with the activated DTPA to form an ester bond. The result of the ^{1}H NMR spectra analysis showed that, the proton peak of COOH–S–S-PTX was changed from δ 2.58 ppm of PTX to δ 2.90 ppm, which is the methylene peak (-CH_2-CH_2-S-S) of DTPA. In addition, the HRMS spectrum analysis of the produced product showed the mass of 1044.3138 ([M − H]- in Supplement Figure 2). Those results together indicate that the PTX-SS-COOH prodrug molecule was successfully synthesized.

2.3. Au@PTXSS-MSN NPs and Au@PTXSS-MSN/DOX@CM NPs preparation and characterization

Followed by the synthesis of the prodrug PTX-S-S-COOH, we then coupled the prodrug to the surface of Au@MSN-NH_2 NPs to gain Au@PTXSS-MSN NPs via condensation reaction, according to a procedure as we have described before [34]. Afterwards, DOX was

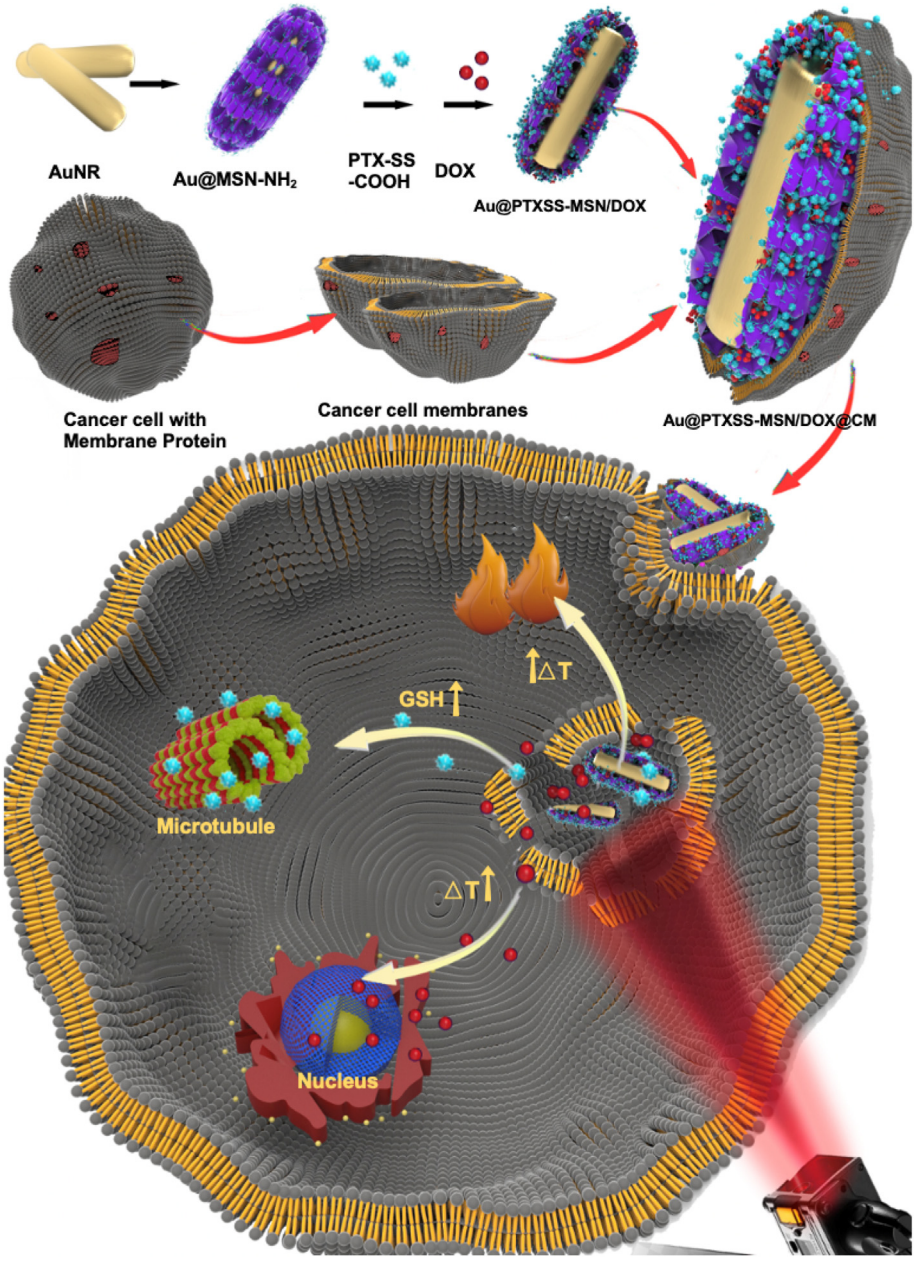

Scheme 1. Schematic representation of Au@PTXSS-MSN/DOX@CM NPs preparation and drug release inside a cell.

further loaded into the Au@PTXSS-MSN NPs for the preparation of Au@PTXSS-MSN/DOX NPs under a mildly agitated conditions. Meanwhile, MDA-MB-231 cells originating cell membranes were coated onto the surface of Au@PTXSS-MSN/DOX NPs to form the final MDA-MB-231 mimicking Au@PTXSS-MSN/DOX@CM NPs (Fig. 1C) by mixing of the aqueous solution of cancer cell membrane, DOX and NPs at 4 °C. This is a very good strategy for the co-delivering of DOX and PTX by one nanocarrier, we have confirmed that drug loading and encapsulation efficiencies of PTX and DOX were 7.2 ± 0.8%, 6.9 ± 1.2% and 77.3 ± 0.6%, 29.8 ± 1.0%, and the drugs loading of DOX and PTX can be controlled at the most efficient mass ratio of 1:1 (Supplementary Figure 5) [34].

As shown in Fig. 1C, a thin layer of cell membrane on the surface of Au@PTXSS-MSN/DOX@CM NPs was obviously observed. The particle size (Fig. 1D) of Au@PTXSS-MSN/DOX NPs were significantly increased up to 123.5 ± 1.2 nm. While the particle size of Au@PTXSS-MSN/DOX@CM NPs was increased up to 141.2 ± 0.8 nm and with the PDI's value of 0.14 ± 0.01 (Supplementary Figure 4B).

2.4. Photothermal performance and DOX release of Au@PTXSS-MSN/DOX@CM NPs in vitro

To further test the photothermal effect of Au@PTXSS-MSN/DOX@CM NPs, we performed the NIR excitation assays. As shown in Fig. 3A and B, the temperature of the NPs dispersed water solution was increased from 30 °C to 60 °C quickly in an intensity and time dependent manner by the irradiate of 980 nm laser with power of 0.5–1 W cm^{-2}. In compared with the NPs dispersed water solution, the temperature of the dilute water solution was slightly changed. These results can well illustrate that the increased temperature of the NPs dispersed water solution is mainly caused by the inner Au NRs of the NPs under the excitation of the laser. The

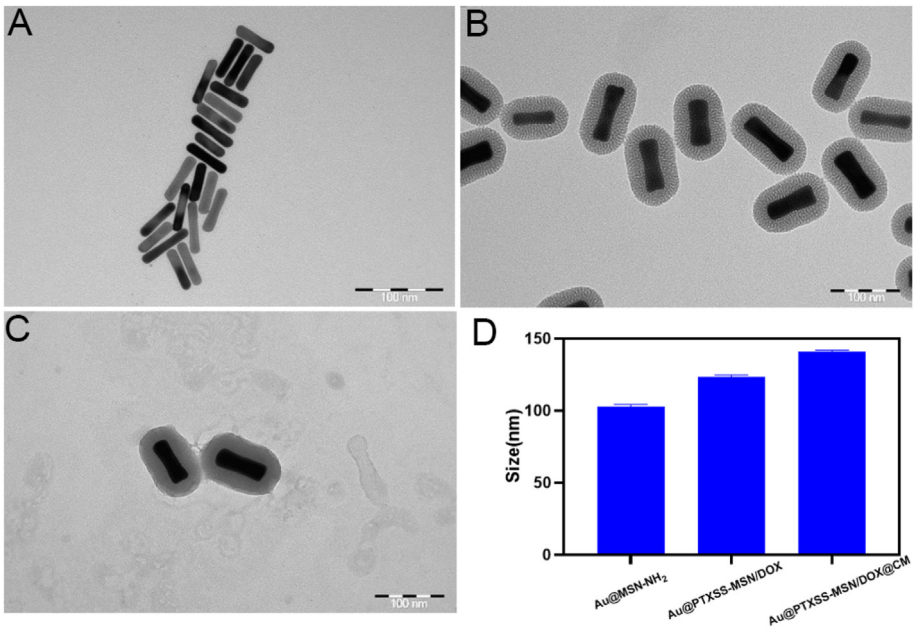

Fig. 1. (**A**–**C**) TEM of AuNRs, Au@MSN-NH_2 NPs and Au@PTXSS-MSN/DOX@CM NPs (scale bar: 100 nm). (**D**) The particle size of each formulations dispersed in deionized water.

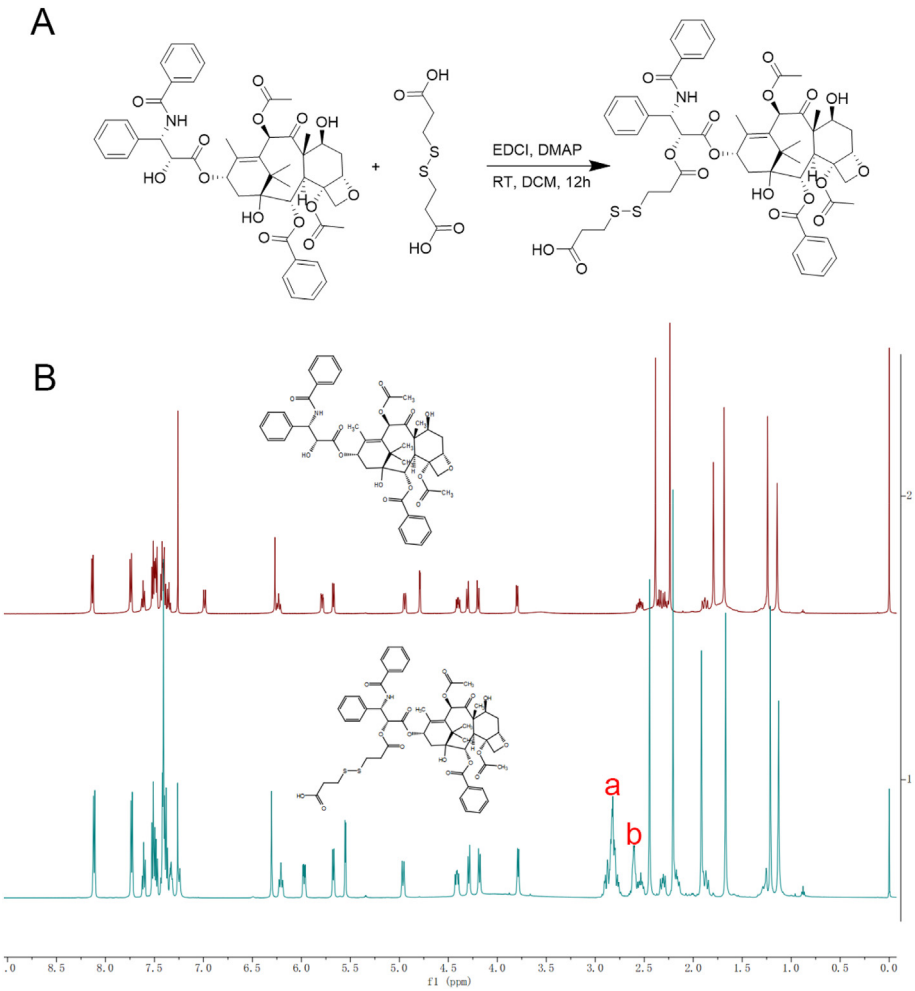

Fig. 2. (**A**) Synthesis route of PTX-S-S-COOH. (**B**) 1H NMR spectra of PTX in $CDCl_3$ and PTX-S-S-COOH in $CDCl_3$.

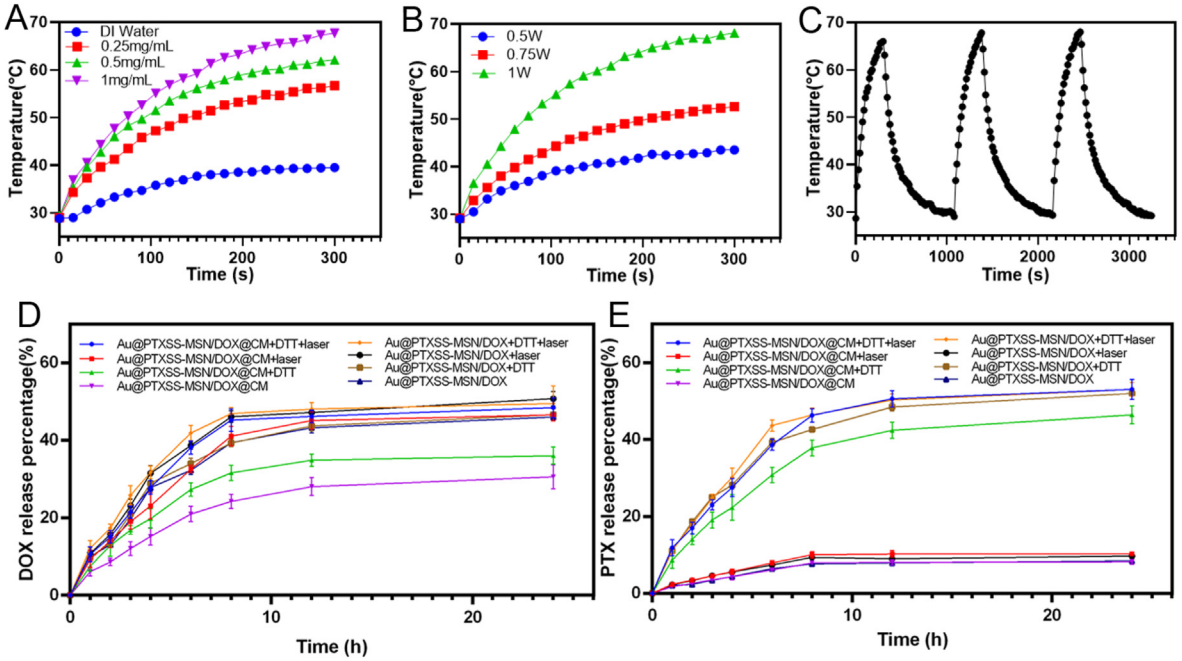

Fig. 3. (**A**) Photothermal heating curves of DI water and Au@PTXSS-MSN/DOX@CM NPs with different NPs concentrations (0.25, 0.5, and 1 mg/mL) under 1.0 W cm^{-2}, 980 nm laser irradiation. (**B**) The temperature profile of Au@PTXSS-MSN/DOX@CM (1 mg/mL) with different laser power intensities (0.5, 0.75, and 1.0 W cm^{-2}, 980 nm). (**C**)Temperature elevation of Au@PTXSS-MSN/DOX@CM NPs (1 mg/mL) over three times of NIR on−off irradiated cycles (1.0 W cm^{-2}, 980 nm). (**D**) DOX and (**E**) PTX Release behavior of Au@PTXSS-MSN/DOX@CM NPs under different conditions.

stability of NPs is one of the most important characters that lead to successfully drug delivery. Therefore, we performed the circulatory laser irradiation assay to test the stability of Au@PTXSS-MSN/DOX@CM NPs. As shown in Fig. 3C, the Au@PTXSS-MSN/DOX@CM NPs exhibited perfect stability under circulatory laser irradiation, because the temperature increasing of Au@PTXSS-MSN/DOX@CM NPs induced by laser irradiation hasn't been changed by three repeated laser irradiations, and the temperature was quickly increased from 28 °C to 67.5 °C within 300 s after each times of laser irradiation. It's reported that increased drug penetration and cell death can be trigged as long as the laser induced temperature goes up to 43 °C [35]. This indicated that synergism between the therapeutical effects of Au@PTXSS-MSN/DOX@CM NPs and photothermal therapy might be achieved.

The drug release is an important indicator to evaluate whether the drug delivery vehicle can be successfully applied. In order to best mimic the intracellular environment i.e. high levels of reducing glutathione (GSH), which is a key factor for the cleavage of disulfide bonds between the PTX and NPs in cancer cells, dithiothreitol (DTT) was added into Au@PTXSS-MSN/DOX@CM NPs dispersed solution as we have described before [36]. The results in Fig. 3 (D and E) and Supplementary Fig. 6 (A and B) show that the DOX release from the Au@PTXSS-MSN/DOX@CM NPs reaches its maximum of 28.0 ± 2.3% at 12 h, and the release was increased up to 34.8 ± 1.6% in the presence of DTT, and the DOX release of only laser group and both DTT and laser groups were 45.1 ± 2.2% and 46.2 ± 1.6%. Since DTT is not a stimulating factor for DOX release, we speculate that the increased DOX release caused by laser is likely to be induced by the breakage of the cell membrane on the surface of the Au@PTXSS-MSN/DOX@CM NPs that was caused by the laser induced temperature change. Meanwhile, the release of PTX was increased from 8.2 ± 0.6% to 46.4 ± 2.3% in the presence of DTT at 24 h. It is very interesting that the laser also increased the release of PTX up to 53.0 ± 2.6% in the present of DTT. All of these results can conclude that laser can significantly increase the release of PTX and DOX from Au@PTXSS-MSN/DOX@CM NPs in the presence of DTT.

2.5. Au@PTXSS-MSN/DOX@CM NPs cytotoxicity and cellular uptake

The cell proliferation inhibition ability of Au@PTXSS-MSN/DOX@CM NPs was measured by WST-1 assay and performed with MCF-10A and MDA-MB-231 cell lines. The results in Fig. 4 (A and B) and Supplementary Figure 6C show that, only the highest concentration of Au@MSN NPs could decrease the proliferation of MCF-10A and MDA-MB-231 cells significantly ($P < 0.05$), indicating that the Au@MSN NPs were slightly or non-cytotoxic within the maximum dose range (10 μg/mL). And the results in MDA-MB-231 cell line (Fig. 4A and B) show that the cell proliferation of the groups treated with the highest concentration of Au@PTXSS-MSN/DOX NPs and Au@PTXSS-MSN/DOX@CM NPs were 49.4 ± 1.0% and 48.2 ± 0.5% ($P > 0.05$), while the laser addition groups were 40.9 ± 2.5% and 29.1 ± 2.1% ($P < 0.001$). Compared with non-laser groups, laser exposure groups were more effective in inhibiting cell proliferation, especially in the highest NPs concentration groups. However, we also noticed that the Au@PTXSS-MSN/DOX@CM NPs haven't show a better ability of cell proliferation inhibition than Au@PTXSS-MSN/DOX NPs. Meanwhile, the result in MCF-10A cell line (Supplementary Fig. 6C) shows that the proliferation ability of cells treated with Au@PTXSS-MSN/DOX@CM NPs was slightly decreased compared to PTX, DOX and PTX-DOX treated groups ($P < 0.01$ in groups of 0.5 μg, 1 μg, 5 μg and 10 μg). Because the cell membrane we have used for the encapsulating of Au@PTXSS-MSN/DOX NPs was derived from MDA-MB-231 cells, this is the main reason that Au@PTXSS-MSN/DOX@CM NPs have a stronger ability of proliferation inhibition in MDA-MB-231 cells than MCF-10A cells. We attribute this difference in proliferation inhibition partially to the passive targeting caused by cell membrane coating induced cell mimicking. While another reason was owing to the higher concentration of GSH that induced more PTX release in breast cancer cell MDA-MB-231 cells than in normal

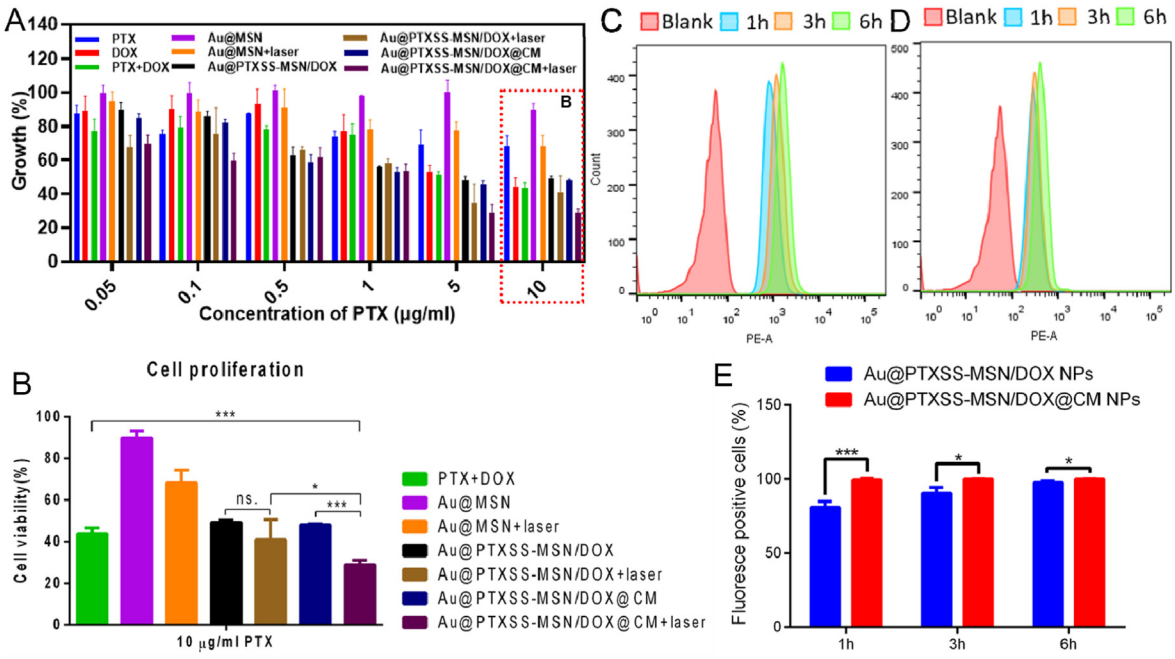

Fig. 4. (**A**) Cell viability of MDA-MB-231 cells after treatment with PTX, DOX, PTX + DOX, Au@MSN NPs, Au@PTXSS-MSN/DOX NPs, and Au@PTXSS-MSN/DOX@CM NPs for 24 h and selectively treated with 980 nm laser irradiation. (**B**) Statistical analyze of MDA-MB-231 cells cell viability after treatment with PTX + DOX, Au@MSN NPs, Au@PTXSS-MSN/DOX NPs, and Au@PTXSS-MSN/DOX@CM NPs for 24 h (concentration selected the highest of 10 μg/mL PTX). Flow cytometry analysis of cellular uptake ability of (C) Au@PTXSS-MSN/DOX@CM and (D) Au@PTXSS-MSN/DOX NPs. (E) Quantification of fluorescence positive cells analyzed by flow cytometry. (Data represent mean ± s.d. (n = 3). sn. represents no significant change, *p < 0.05, **p < 0.01 and ***p < 0.001).

mammary gland cell MCF-10A cells.

To verify the existence of this passive targeting effect, we performed flow cytometry analysis and confocal microscope imaging assays to measure the Au@PTXSS-MSN/DOX@CM NPs cellular uptake. The result in Fig. 4 show that the DOX positive cells in Au@PTXSS-MSN/DOX@CM NPs (Fig. 4C) and Au@PTXSS-MSN/DOX NPs treated MDA-MB-231 cells (Fig. 4D) were 96.7 ± 2.1% and 83.3 ± 3.2% at the time point of 1 h. And the detected fluorescence of DOX were obviously decreased in Au@PTXSS-MSN/DOX NPs treated MCF-10A cells (Supplementary Fig. 7A and B). We then labeled the cell membrane of the Au@PTXSS-MSN/DOX@CM NPs with 3,3′-dioctadecyloxacarbocyanine perchlorate (Dio), which is a green fluorescent dye that can selectively bind to the cell membrane. As shown in Fig. 5A, the green fluorescent signal of Dio and the DOX red fluorescent signal have a very obvious co-localization in the cell. And compared to the non-cell membrane coated Au@PTXSS-MSN/DOX NPs treated group (Fig. 5B), a very obviously DOX red fluorescent signal can be observed in the cell nucleus of MDA-MB-231 cells treated with Au@PTXSS-MSN/DOX@CM NPs at 3 and 6 h, while the DOX red fluorescent signal in the cell nucleus only can be observed at 6 h in Au@PTXSS-MSN/DOX@CM NPs treated group. All of these results indicated that Au@PTXSS-MSN/DOX@CM NPs have a better cellular uptake and earlier DOX release than Au@PTXSS-MSN/DOX NPs in the co-incubation with MDA-MB-231 cells.

2.6. Lysosomal escape of Au@Cy5.5-MSN@CM NPs

The endo/lysosome trap has always been considered as the main problem that lead to the failure of intracellular drug delivery [37]. We have shown that laser has the ability of promoting the release of DOX and PTX from Au@PTXSS-MSN/DOX@CM NPs (Fig. 3D and E and Supplementary Fig. 6A and B), and also enhance the ability of cell proliferation inhibition by Au@PTXSS-MSN/DOX@CM NPs (Fig. 4A and B). We thus hypothesize that the laser induced temperature increasing might have a promoting effect on the Au@PTXSS-MSN/DOX@CM NPs' lysosomal escape. In order to verify this hypothesis, we labeled the Au@MSN@CM NPs with a red fluorescent dye Cy5.5, while green fluorescent lysosome tracker has been used for the lysosome labeling. The results in Fig. 6A and B shows that, most of the red fluorescent signal that represents Au@Cy5.5-MSN@CM NPs were localized together with green fluorescent signal that represents the lysosome in the Au@Cy5.5-MSN@CM NPs treated group. However, the overlap of red fluorescent signal and green fluorescent signal were significantly decreased from 71.4% to 42.6% in the presence of laser treatment after 4 h co-incubation with Au@Cy5.5-MSN@CM NPs, especially after 6 h (the overlap were decreased from 68.7% to 30.8%). These results indicated that, the Au@Cy5.5-MSN@CM NPs were more able to get outside of the lysomes under laser condition. Therefore, we have confirmed that the photothermal effect of Au@Cy5.5-MSN@CM NPs shows potential in the promoting lysosomal escape of Au@MSN@CM NPs. And this promoting effect may be contributing to the destructive effect of photothermal therapy on the biofilms [35].

2.7. Antitumor activity in vivo

Previously, we have shown that the laser irradiation have a synergetic effect in the promoting of Au@Cy5.5-MSN@CM NPs lysosomal escaping and also can increase the proliferation inhibition ability of Au@PTXSS-MSN@CM NPs against MDA-MB-231 cells. Subsequently, we further tested the biodistribution and antitumor activity of Au@PTXSS-MSN/DOX@CM NPs in 4T1 breast cancer cell line formed tumor burden mouse model in combination with photothermal therapy. Compared to the DOX treated group, DOX signal was mainly detected in the tumor site after 24 h treatment of Au@PTXSS-MSN/DOX@CM NPs (Supplementary Figure 8).

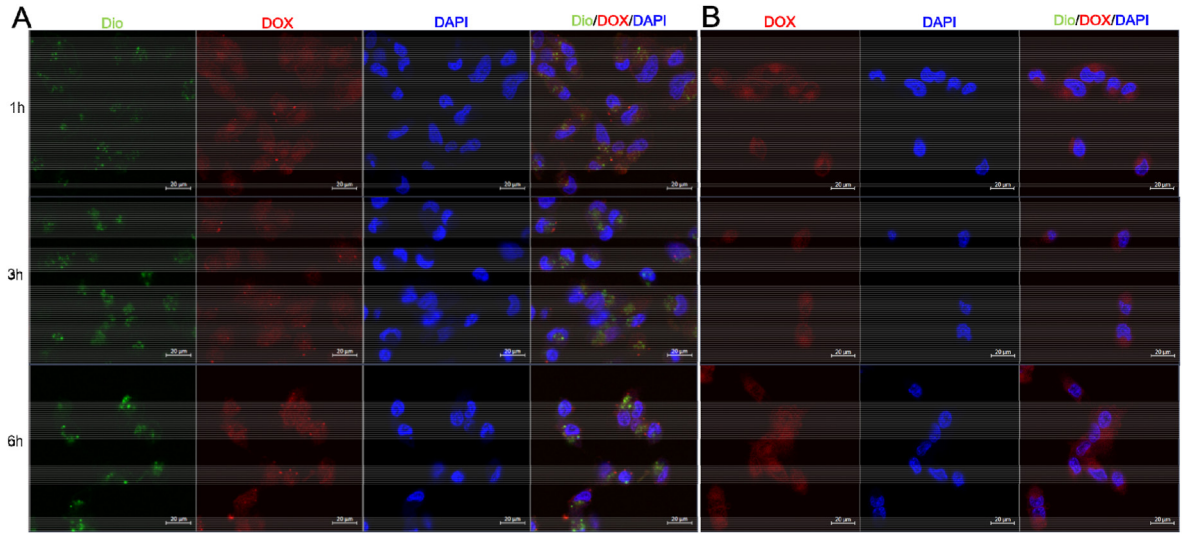

Fig. 5. Fluorescence images of MDA-MB-231 cells incubated with (**A**) Au@PTXSS-MSN/DOX@CM and (**B**) Au@PTXSS-MSN/DOX for 1–6 h (Blue channel: DAPI; Red channel: DOX; Green channel: DIO; Scale bar: 20 μm).

Considering the proper particle size of Au@PTXSS-MSN/DOX@CM NPs, we attribute this preferred accumulation of Au@PTXSS-MSN/DOX@CM NPs at tumor site to the ERP effect of NPs. And finally, as shown in Fig. 7 (A and **C**), the tumor growth has been significantly suppressed by Au@PTXSS-MSN/DOX@CM NPs compared to the PBS and PTX + DOX treated groups ($p < 0.001$). However, the combined Au@PTXSS-MSN/DOX@CM NPs with laser treatment did not exhibits a better antitumor effect than Au@PTXSS-MSN/DOX@CM NPs only group ($p = 0.877$). We consider this may be due to the failure of laser irradiation control and the weak skin penetration ability of laser irradiation. Surprisingly, we also noticed that the tumor growth in PTX + DOX treated group did not show a significant growth suppression compared to PBS control group. We attribute this result to the lipophilicity of PTX, because effective PTX penetration to the tumor site cannot be easily achieved by intravenous injection. Besides, low concentration of DOX (5 mg/kg) may be another reason for the poor antitumor activity of PTX + DOX treated group, because the predicted doxorubicin-induced cardiac toxicity [38] have not been observed in the results of HE staining (Supplementary Figure 9).

3. Conclusion

In summary, we have developed a new photothermal and GSH responsive NP with cell camouflage for targeted TNBC therapy. The Au NRs were embedded into the Au@PTXSS-MSN/DOX@CM with photothermal therapy activity, while the porous shell structure formed by MSN realized the high drug loading capacity to load the hydrophilic DOX. The prodrug technology enabled the PTX prodrug to have a GSH responsive linker and a conjugation site for conjugating onto the MSN. The coated cell membrane originating from tumor cells can protect the drugs from premature releasing and greatly improved the tumor targeting efficiency. Au@PTXSS-MSN/DOX@CM NPs have been confirmed to have good tumor cell targeting and synergistic anti-tumor effects at the cellular level. In addition, the Au@PTXSS-MSN/DOX@CM NPs also generated significant anti-tumor activity *in vivo*, as well as further improve the on-site drug release, for targeted TNBC therapy. Although the combination of Au@PTXSS-MSN/DOX@CM NPs and photothermal therapy haven't exhibited a better anti-tumor activity than Au@PTXSS-MSN/DOX@CM NPs only groups *in vivo*, it offers a good inspiration for combination therapy of TNBC.

4. Methods and materials

4.1. Materials

Paclitaxel (PTX), Doxorubicin (DOX), *N*-(3-dimethylaminopropyl)-*N*-ethylcarbodiimide hydrochloride (EDC·HCl), 3,3′-Dithiodipropionic acid (DTDP), and 4-dimethylaminopyridine (DMAP) were all purchased from Tansoole (China). 3,3′-dioctadecyloxacarbocyanine perchlorate (DIO) were purchased from Shanghai Maokang biotechnology Co., Ltd (China). Sodium borohydride ($NaBH_4$), tetraethyl orthosilicate (TEOS), silver nitrate ($AgNO_3$), ascorbic acid, tetrachloroauric acid ($HAuCl_4$), cetyltrimethyl ammonium bromide (CTAB), DL-Dithiothreitol (DTT), 4′,6′-diamidine-2′-phenylindole (DAPI), dichloromethane (DCM) and menthol (MeOH) were purchased from Sigma-Aldrich (Finland).

4.2. Cell lines and cell culture

MCF-10A and MDA-MB-231 cell lines were purchased from American Type Culture Collection (ATCC, Manassas, VA, USA) and maintained at 37 °C with 5% CO_2. MDA-MB-231 cell line was cultured in DMEM medium (LONZA) and 10% FBS and 1% PS (penicillin and streptomycin solution) were added. MCF-10A cell line was cultured in DMED F12 medium (LONZA) and 10% of horse serum (LONZA), 20 ng/mL epidermal growth factor, 100 ng/mL cholera toxin, 0.16 Units/ml insulin, 500 ng/mL hydrocortisone and 1% PS were added.

4.3. Synthesis of AuNRs

The CTAB solution (7.5 mL, 0.1 M) and $HAuCl_4$ solution (0.25 mL, 0.01 M) were mixed for 5 min. Afterwards, 0.6 mL ice-cold $NaBH_4$ solution (0.01 M) was injected into the mixture rapidly under vigorous stirring and the gold seeds were formed. Four hours later, a solution consisting of 400 mL CTAB (0.1 M), 20 mL $HAuCl_4$ (0.01 M), 4.8 mL $AgNO_3$ (0.01 M) and 7.6 mL HCl (1 M) was stirred at 30 °C for 10 min. And 4 mL ascorbic acid (0.1 M) was quickly added into the growth solution, and the solution immediately becomes colorless. Finally, the prepared gold seeds (0.96 mL) solution were

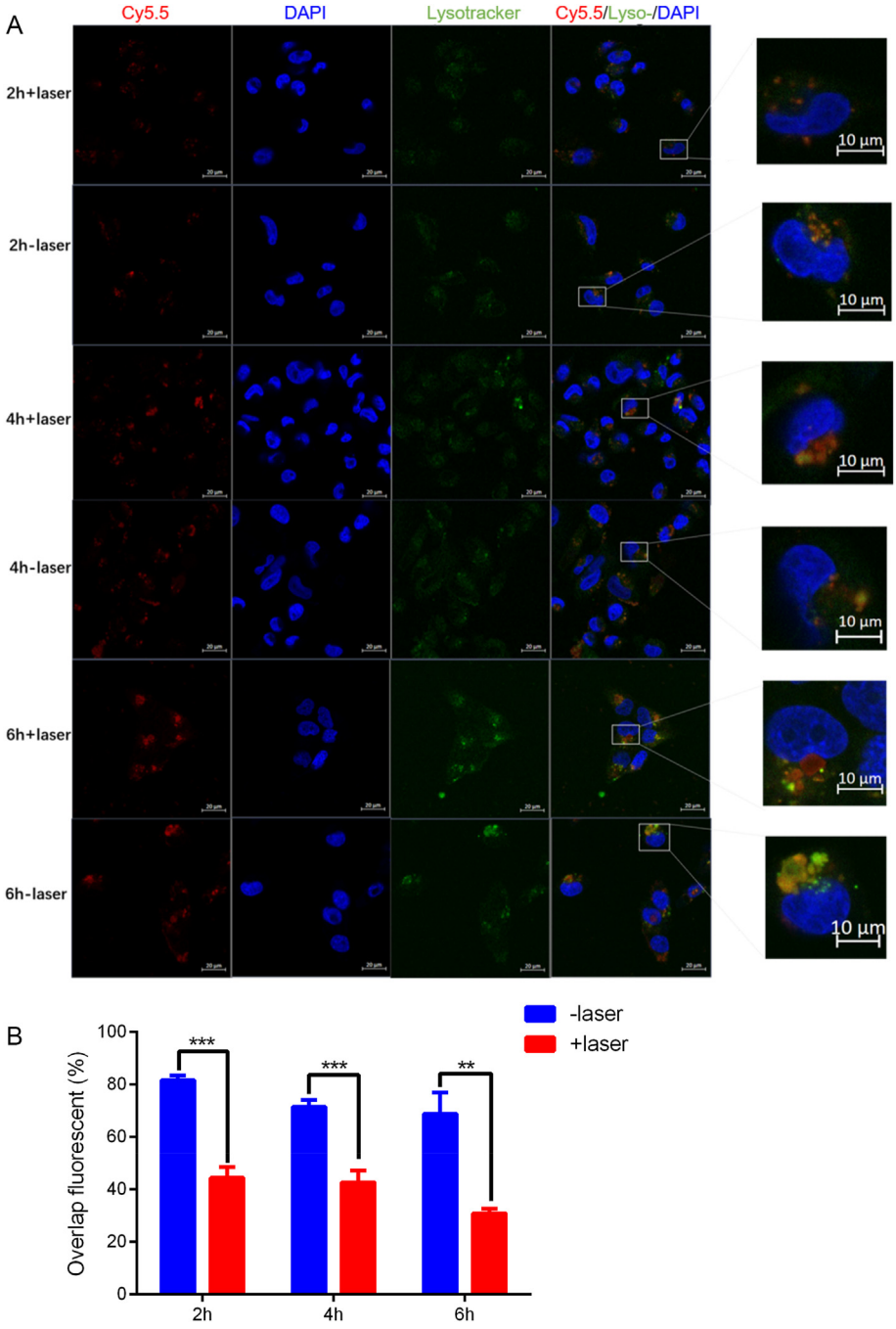

Fig. 6. Endosomal escape analysis of the intracellular uptaken Au@Cy5.5-MSN@CM NPs in MDA-MB-231 cells. A. Confocal microscopy images after cells culturing with Au@Cy5.5-MSN@CM NPs for 2 h, 4 h, and 6 h. And cells were selectively treated with laser for 5 min (Blue channel: DAPI; Red channel: Cy5.5; Green channel: lysotracker; Scale bar: 20 μm). B. Quantified co-localization of Cy5.5 and Lysotracker by Image J software. (3 images from each group were used for overlap fluorescence analysis).

added and stirred for 5 more minutes, then left for overnight.

4.4. Synthesis of Au@MSN-NH_2 NPs

First, purified AuNRs were transferred to aqueous CTAB solution (50 mL, 1 mM) and then adjust the alkalinity of the solution to pH 10–11 with 0.1 M NaOH. Next, 0.33 mL of 20 v/v% TEOS ethanol solution was added, and the mixture was left to react for overnight at 30 °C. The synthesized Au@MSN NPs were collected by 10 min centrifuge at 13000 rpm and then washed with 0.6 wt % ammonium nitrate (NH_4NO_3) ethanol solution to remove CTAB. Finally, the Au@MSN NPs were modified into an activated form of Au@MSN-NH_2 NPs by APTES in ethanol for overnight.

4.5. Synthesis of PTX-S-S-COOH

Briefly, PTX (1.0 g), DTDP (295.47 mg), EDCI (268.51 mg) and DMAP (171.68 mg) were firstly added into 20 mL of dichloromethane, and stirred to reaction for overnight at room temperature. And next, purify the crude product with silica gel column chromatography to for the pure intermediate (yield = 59%).

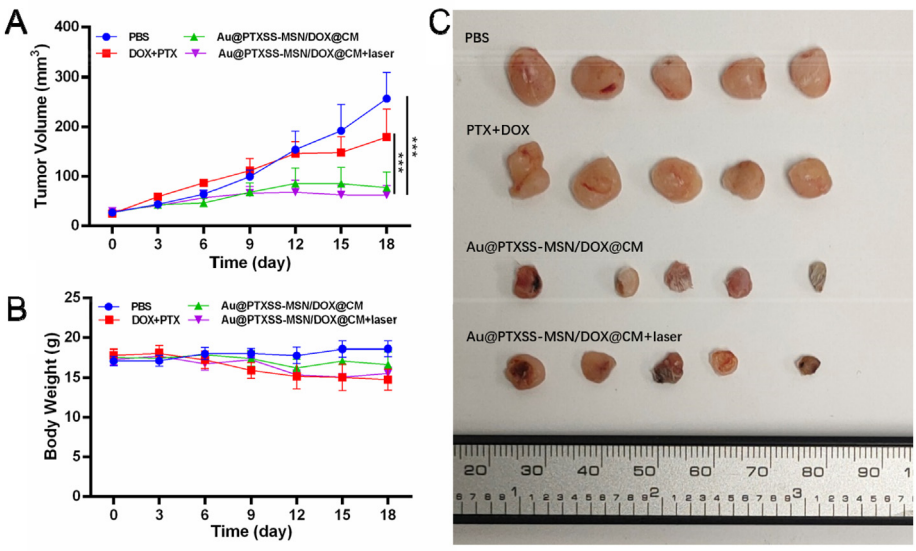

Fig. 7. Results of antitumor efficacy of Au@PTXSS-MSN/DOX@CM NPs *in vivo*. Recorded tumor volumes (A), body weight (B), and photograph of isolated tumors from 4T1-tumor burden mice (C).

4.6. Synthesis of Au@PTXSS-MSN and drug loading

Au@MSN-NH_2 were dispersed in a dichloromethane solution of PTX-SS-COOH, DMAP, EDCI at room temperature and stirred overnight. Wash the NPs with excess dichloromethane. The prodrug-modified Au@PTXSS-MSN were then stirred with DOX aqueous solution overnight to complete the DOX loading.

4.7. MSC membrane preparation and preparation of MSN@M

MDA-MB-231 cells were collected, washed three times with PBS and then incubated in Tris buffer containing 10 mM Tris, 10 mM $MgCl_2$ and protease inhibitor for 1 h at 4 °C and sonicated for 10 min in an ice bath. Cell membrane fragments were obtained by differential centrifugation of the homogenate on the broken cells, first at 500 g, centrifuged for 10 min, the precipitate was discarded and the supernatant was retained, then the supernatant was centrifuged for 10 min at 10,000 g and the supernatant was lyophilized to obtain cancer cell membranes. Then the aqueous solution of cancer cell membrane and DOX was mixed with NPs at 4 °C, stirred overnight, and centrifuged to obtain Au@PTXSS-MSN/DOX@CM.

4.8. Characterization of the PTX-S-S-COOH prodrug

The mass spectra results of PTX-S-S-COOH and PTX were measured with a Bruker Daltonics microTOF-Q mass spectrometer (Bruker, Billerica, MA, USA). And ^1H NMR spectra results were analyzed by Bruker 500 NMR spectrometers (Bruker, Billerica, MA, USA).

4.9. Measurement of photothermal performance

Three experiments were performed to measure the photothermal conversion capacity of Au@PTXSS-MSN/DOX@CM NPs. Temperature tests were performed on 1 mL of aqueous solutions of NPs with different concentrations (0, 0.25, 0.5 and 1 mg/mL). Then, 1 mL of aqueous NPs with the same concentration (1 mg/mL) was used and irradiated for 300s at the power densities of 0.5–1 W/cm^{-2}. A third experiment was performed by using 1 mg/mL NPs/DOX solution and irradiating it with 1 W/cm^{-2}. The experiment was repeated three times by heating with a 1 mg/mL NPs/DOX solution and 1 W/cm^{-2} NIR laser, and followed by cooling to room temperature in natural state. The temperature was recorded every 15s by the thermal imaging camera.

4.10. Drug release behavior

Cumulative levels of DOX and PTX release from NPs were determined using a dialysis method. 1 mL of each NPs were added in a dialysis bag (MW: 3500) and placed in a PBS solution containing 0.5% Tween 80 with or without DTT (10 mM). The solution is placed in a 37 °C constant temperature shaker and shaken horizontally. 1 mL of the incubation solution was removed and supplemented with an equal volume at each predetermined time point. The laser group was irradiated with a 1 W/cm^{-2} IR laser for 5 min at each time point. DOX and PTX concentration in the solution were measured by HPLC.

4.11. Cellular uptake and lysosomal escape assay

Au@PTXSS-MSN/DOX@CM NPs cellular uptake was performed in MCF-10A cells and MDA-MB-231. Briefly, cells were seeded into 6-well plate or confocal dish at the density of 1.8–2 × 10^5/well. 24 h later, the cells were cultured with 2 mL fresh medium contains Au@PTXSS-MSN/DOX@CM NPs (equal to 10 μg/mL DOX) for 1–6 h. After that, the culture medium were discard and fixed with 4% PFA and followed by 0.5 μg/mL DAPI staining for 5 min. The cell imaging were taken with Zeiss LSM880 confocal microscope, cellular uptake and flow cytometry assay were performed with BD LSRFortessa.

NPs lysosome escape assay was performed in MDA-MB-231 cells, cells were selectively treated with Au@Cy5.5-MSN@CM NPs and laser for 2–6 h in confocal dishes. And followed the cell culture medium were replaced with fresh cell culture medium contains Lysosome Tracker were added for 3 more hours. Finally, the cells were fixed with 4% PFA and followed by 0.5 μg/mL DAPI staining for 5 min.

4.12. In vitro cytotoxicity assay

Cytotoxicity were evaluated by cell proliferation inhibition and measured by WST-1 assay. Briefly, MDA-MB-231 cells and MCF-10A cells were seeded in 96-well plate at the density of 4000–5000 per well. The day next, PTX、DOX、PTX + DOX、Au@MSN NPs、Au@PTXSS-MSN/DOX NPs and Au@PTXSS-MSN/DOX@CM NPs were added into the cell culture medium, and cells were selectively treated with 980 nm laser with power of 1 W/cm^{-2} for 5 min after 12 h co-incubation. And 12 h later, WST-1 were added in the cell culture medium and incubated at 5% CO_2 37 °C for 2 h, and finally OD's value at 450 nm were measured with Thermo Varioskanflash.

4.13. Animal study

All experiments including animal operations were approved by the Animal Research Committee of Jiangsu University, China (SCXK (Jiangsu)-2018-0012). Matrigel and 5000 4T1 cells were mixed and injected into the axillary fat pads of 8-week-old female nude mice. The tumor burden mice were randomly divided into 4 groups and injected with 100 μl PBS, PTX + DOX (5 mg/kg of each) or Au@PTXSS-MSN/DOX@CM NPs (equal to 5 mg/kg DOX + PTX) from the tail vain every three days. And the mice of one Au@PTXSS-MSN/DOX@CM NPs injected group were treated with 980 nm laser with the power of 1 W/cm^{-2} for 5 min the day next of each injection. The tumor growth and body weight were recorded. And all of the mice were sacrificed after 6 times injection, the tumor tissues and main organs (heart, liver, spleen, lung and kidney) were collected and fixed with 4% PFA for further HE staining.

4.14. Statistical data analysis

All of the data were collected from triplicated independent assays. Data are analyzed with the student's t-test and shown as means ± SD. GraphPad, Image J and SPSS 20.0 Software (IBM Inc., Armonk, NY, USA) were used for all statistical analyses. *P*-values < 0.05 were considered significant.

Credit author statement

Lirong Zhang: Cell experiment operator, Project design, manuscript writing and reviewing. **Xiaodong Ma:** Project design, Nanoparticle preparation and chart drawing. **Wenhui Zhou:** Cell experiment operator, Editing and Reviewing the entire manuscript. **Qiwei Wu:** Animal experimental operator. **Jiaqi Yan:** Schematic drawing and manuscript editing. **Xiaoyu Xu:** Analyzing data of cell experiment. **Bhawana Ghimire:** Assist in the preparation of nanoparticles. **Jessica M. Rosenholm:** Support the supervision of the project and writings polishing. **Jing Feng:** Supervision, reviewing of whole manuscript, focusing on key issues related to cell study. **Dongqing Wang:** Supervision, reviewing of whole manuscript, focusing on key issues related to animal study. **Hongbo Zhang:** Supervision, reviewing of whole manuscript, focusing on key issues related to different nanoparticle formulations. Funding acquirement.

Declaration of competing interest

The authors declare that they have no known competing financial interests or personal relationships that could have appeared to influence the work reported in this paper.

Acknowledgements

Imaging/Flow cytometry was performed at the Cell Imaging and Cytometry core at Turku Bioscience Centre, which is supported by Biocenter Finland. This work was financially supported by Jiangsu Provincial Key Research and Development Programme (Grant No. BE2018690), Distinguished Clinical Investigator Grant of Jiangsu Province (JSTP201701), Program for Outstanding Medical Academic Leader of Shanghai (LJ2019025), the Key Subject Construction Project for Medical of Shanghai (ZK2019B29) and Academy of Finland (328933). This work is also part of the activities within the strategic research profiling area Solutions for Health at Åbo Akademi University (Academy of Finland, # 336355).

Appendix A. Supplementary data

Supplementary data to this article can be found online at https://doi.org/10.1016/j.mtadv.2021.100199.

References

[1] G. Bianchini, J.M. Balko, I.A. Mayer, M.E. Sanders, L. Gianni, Triple-negative breast cancer: challenges and opportunities of a heterogeneous disease, Nat. Rev. Clin. Oncol. 13 (2016) 674–690, https://doi.org/10.1038/nrclinonc.2016.66.
[2] L. Yin, J.J. Duan, X.W. Bian, S.C. Yu, Triple-negative breast cancer molecular subtyping and treatment progress, Breast Cancer Res. 22 (2020) 61, https://doi.org/10.1186/s13058-020-01296-5.
[3] P. Chowdhury, U. Ghosh, K. Samanta, M. Jaggi, S.C. Chauhan, M.M. Yallapu, Bioactive nanotherapeutic trends to combat triple negative breast cancer, Bioac.t Mater. 6 (2021) 3269–3287, https://doi.org/10.1016/j.bioactmat.2021.02.037.
[4] Z. He, Y. Zhang, N. Feng, Cell membrane-coated nanosized active targeted drug delivery systems homing to tumor cells: a review, Mat. Sci. Eng. C Mat. Bio.l Appl. 106 (2020) 110298, https://doi.org/10.1016/j.msec.2019.110298.
[5] D. Nie, Z. Dai, J. Li, Y. Yang, Z. Xi, J. Wang, W. Zhang, K. Qian, S. Guo, C. Zhu, R. Wang, Y. Li, M. Yu, X. Zhang, X. Shi, Y. Gan, Cancer-cell-membrane-coated nanoparticles with a yolk-shell structure augment cancer chemotherapy, Nano Lett. 20 (2020) 936–946, https://doi.org/10.1021/acs.nanolett.9b03817.
[6] H. Sun, J. Su, Q. Meng, Q. Yin, L. Chen, W. Gu, P. Zhang, Z. Zhang, H. Yu, S. Wang, Y. Li, Cancer-cell-biomimetic nanoparticles for targeted therapy of homotypic tumors, Adv. Mater. 28 (2016) 9581–9588, https://doi.org/10.1002/adma.201602173.
[7] J. Rautio, H. Kumpulainen, T. Heimbach, R. Oliyai, D. Oh, T. Jarvinen, J. Savolainen, Prodrugs: design and clinical applications, Nat. Rev. Drug Discov. 7 (2008) 255–270, https://doi.org/10.1038/nrd2468.
[8] J. Rautio, N.A. Meanwell, L. Di, M.J. Hageman, The expanding role of prodrugs in contemporary drug design and development, Nat. Rev. Drug Discov. 17 (2018) 559–587, https://doi.org/10.1038/nrd.2018.46.
[9] R. Walther, J. Rautio, A.N. Zelikin, Prodrugs in medicinal chemistry and enzyme prodrug therapies, Adv. Drug Deliv. Rev. 118 (2017) 65–77, https://doi.org/10.1016/j.addr.2017.06.013.
[10] W.C. Geng, J.L. Sessler, D.S. Guo, Supramolecular prodrugs based on host-guest interactions, Chem. Soc. Rev. 49 (2020) 2303–2315, https://doi.org/10.1039/c9cs00622b.
[11] L. Hao, Q. Zhou, Y. Piao, Z. Zhou, J. Tang, Y. Shen, Albumin-binding prodrugs via reversible iminoboronate forming nanoparticles for cancer drug delivery, J. Contr. Release 330 (2021) 362–371, https://doi.org/10.1016/j.jconrel.2020.12.035.
[12] N. Hattori, M. Sako, K. Kimura, N. Iida, H. Takeshima, Y. Nakata, Y. Kono, T. Ushijima, Novel prodrugs of decitabine with greater metabolic stability and less toxicity, Clin. Epigenet. 11 (2019) 111, https://doi.org/10.1186/s13148-019-0709-y.
[13] P.E. Saw, H. Yao, C. Lin, W. Tao, O.C. Farokhzad, X. Xu, Stimuli-responsive polymer-prodrug hybrid nanoplatform for multistage siRNA delivery and combination cancer therapy, Nano Lett. 19 (2019) 5967–5974, https://doi.org/10.1021/acs.nanolett.9b01660.
[14] M. Umeh-Garcia, C. Simion, P.Y. Ho, N. Batra, A.L. Berg, K.L. Carraway, A. Yu, C. Sweeney, A novel bioengineered miR-127 prodrug suppresses the growth and metastatic potential of triple-negative breast cancer cells, Cancer Res. 80 (2020) 418–429, https://doi.org/10.1158/0008-5472.CAN-19-0656.
[15] C. Yang, K. Tu, H. Gao, L. Zhang, Y. Sun, T. Yang, L. Kong, D. Ouyang, Z. Zhang, The novel platinum(IV) prodrug with self-assembly property and structure-transformable character against triple-negative breast cancer, Biomaterials 232 (2020) 119751, https://doi.org/10.1016/j.biomaterials.2019.119751.
[16] Y. Liu, P. Bhattarai, Z. Dai, X. Chen, Photothermal therapy and photoacoustic imaging via nanotheranostics in fighting cancer, Chem. Soc. Rev. 48 (2019) 2053–2108, https://doi.org/10.1039/c8cs00618k.
[17] X. Li, J.F. Lovell, J. Yoon, X. Chen, Clinical development and potential of photothermal and photodynamic therapies for cancer, Nat. Rev. Clin. Oncol. 17 (2020) 657–674, https://doi.org/10.1038/s41571-020-0410-2.
[18] N. Gupta, R. Malviya, Understanding and advancement in gold nanoparticle

targeted photothermal therapy of cancer, Biochim. Biophys. Acta Rev. Canc (2021) 188532, https://doi.org/10.1016/j.bbcan.2021.188532, 1875.
[19] Z.J. Zhao, J. Gong, Golden touch of the nanoparticles, Nat. Nanotechnol. 15 (2020) 1–2, https://doi.org/10.1038/s41565-020-0740-3.
[20] E. Boisselier, D. Astruc, Gold nanoparticles in nanomedicine: preparations, imaging, diagnostics, therapies and toxicity, Chem. Soc. Rev. 38 (2009) 1759–1782, https://doi.org/10.1039/b806051g.
[21] P. Singh, S. Pandit, V. Mokkapati, A. Garg, V. Ravikumar, I. Mijakovic, gold nanoparticles in diagnostics and therapeutics for human cancer, Int. J. Mol. Sci. 19 (2018), https://doi.org/10.3390/ijms19071979.
[22] Y. Zhou, G. Quan, Q. Wu, X. Zhang, B. Niu, B. Wu, Y. Huang, X. Pan, C. Wu, Mesoporous silica nanoparticles for drug and gene delivery, Acta Pharm. Sin. B 8 (2018) 165–177, https://doi.org/10.1016/j.apsb.2018.01.007.
[23] A. Barkat, S. Beg, S.K. Panda, S.A. K, M. Rahman, F.J. Ahmed, Functionalized mesoporous silica nanoparticles in anticancer therapeutics, Semin. Cancer Biol. 69 (2021) 365–375, https://doi.org/10.1016/j.semcancer.2019.08.022.
[24] T.L. Nguyen, Y. Choi, J. Kim, Mesoporous silica as a versatile platform for cancer immunotherapy, Adv. Mater. 31 (2019), e1803953, https://doi.org/10.1002/adma.201803953.
[25] A. Hernandez Montoto, A. Llopis-Lorente, M. Gorbe, M.T. J, R. Cao-Milan, B. Diaz de Grenu, M. Alfonso, J. Ibanez, M.D. Marcos, M. Orzaez, R. Villalonga, R. Martinez-Manez, F. Sancenon, Janus gold nanostars-mesoporous silica nanoparticles for NIR-light-triggered drug delivery, Chemistry 25 (2019) 8471–8478, https://doi.org/10.1002/chem.201900750.
[26] B.S. Kim, Y.T. Chen, P. Srinoi, M.D. Marquez, T.R. Lee, Hydrogel-encapsulated mesoporous silica-coated gold nanoshells for smart drug delivery, Int. J. Mol. Sci. 20 (2019), https://doi.org/10.3390/ijms20143422.
[27] A. Hernandez Montoto, R. Montes, A. Samadi, M. Gorbe, J.M. Terres, R. Cao-Milan, E. Aznar, J. Ibanez, R. Masot, M.D. Marcos, M. Orzaez, F. Sancenon, L.B. Oddershede, R. Martinez-Manez, Gold nanostars coated with mesoporous silica are effective and nontoxic photothermal agents capable of gate keeping and laser-induced drug release, ACS Appl. Mater. Interfaces 10 (2018) 27644–27656, https://doi.org/10.1021/acsami.8b08395.
[28] C.J. Murphy, H.H. Chang, P. Falagan-Lotsch, M.T. Gole, D.M. Hofmann, K.N.L. Hoang, S.M. McClain, S.M. Meyer, J.G. Turner, M. Unnikrishnan, M. Wu, X. Zhang, Y. Zhang, Virus-sized gold nanorods: plasmonic particles for biology, Acc. Chem. Res. 52 (2019) 2124–2135, https://doi.org/10.1021/acs.accounts.9b00288.
[29] G. Yu, B. Zhu, L. Shao, J. Zhou, M.L. Saha, B. Shi, Z. Zhang, T. Hong, S. Li, X. Chen, P.J. Stang, Host-guest complexation-mediated codelivery of anticancer drug and photosensitizer for cancer photochemotherapy, Proc. Natl. Acad. Sci. U. S. A. 116 (2019) 6618–6623, https://doi.org/10.1073/pnas.1902029116.
[30] M.M. Khan, N. Filipczak, V.P. Torchilin, Cell penetrating peptides: a versatile vector for co-delivery of drug and genes in cancer, J. Contr. Release 330 (2021) 1220–1228, https://doi.org/10.1016/j.jconrel.2020.11.028.
[31] M.D. Zhao, J.Q. Li, F.Y. Chen, W. Dong, L.J. Wen, W.D. Fei, X. Zhang, P.L. Yang, X.M. Zhang, C.H. Zheng, Co-delivery of curcumin and paclitaxel by "Core-Shell" targeting amphiphilic copolymer to reverse resistance in the treatment of ovarian cancer, Int. J. Nanomed. 14 (2019) 9453–9467, https://doi.org/10.2147/IJN.S224579.
[32] G. Liang, Y. Zhu, D.J. Ali, T. Tian, H. Xu, K. Si, B. Sun, B. Chen, Z. Xiao, Engineered exosomes for targeted co-delivery of miR-21 inhibitor and chemotherapeutics to reverse drug resistance in colon cancer, J. Nanobiotechnol. 18 (2020) 10, https://doi.org/10.1186/s12951-019-0563-2.
[33] S. Joshi, M.T. Hussain, C.B. Roces, G. Anderluzzi, E. Kastner, S. Salmaso, D.J. Kirby, Y. Perrie, Microfluidics based manufacture of liposomes simultaneously entrapping hydrophilic and lipophilic drugs, Int. J. Pharm. 514 (2016) 160–168, https://doi.org/10.1016/j.ijpharm.2016.09.027.
[34] J. Yan, X. Xu, J. Zhou, C. Liu, L. Zhang, D. Wang, F. Yang, H. Zhang, Fabrication of a pH/redox-triggered mesoporous silica-based nanoparticle with microfluidics for anticancer drugs doxorubicin and paclitaxel codelivery, Acs Appl. Bio Mater. 3 (2020) 1216–1225, https://doi.org/10.1021/acsabm.9b01111.
[35] G.M. Hahn, J. Braun, I. Har-Kedar, Thermochemotherapy: synergism between hyperthermia (42-43 degrees) and adriamycin (of bleomycin) in mammalian cell inactivation, Proc. Natl. Acad. Sci. U. S. A. 72 (1975) 937–940, https://doi.org/10.1073/pnas.72.3.937.
[36] X. Ma, E. Ozliseli, Y. Zhang, G. Pan, D. Wang, H. Zhang, Fabrication of redox-responsive doxorubicin and paclitaxel prodrug nanoparticles with microfluidics for selective cancer therapy, Biomater. Sci. 7 (2019) 634–644, https://doi.org/10.1039/c8bm01333k.
[37] L. Wu, W. Zhou, L. Lin, A. Chen, J. Feng, X. Qu, H. Zhang, J. Yue, Delivery of therapeutic oligonucleotides in nanoscale, Bioact. Mat. (2021), https://doi.org/10.1016/j.bioactmat.2021.05.038.
[38] M. Namdari, A. Eatemadi, Cardioprotective effects of curcumin-loaded magnetic hydrogel nanocomposite (nanocurcumin) against doxorubicin-induced cardiac toxicity in rat cardiomyocyte cell lines, Artif Cells Nanomed Biotechnol. 45 (2017) 731–739, https://doi.org/10.1080/21691401.2016.126103.